First principles study of lithium insertion in bulk silicon

2010 J. Phys.: Condens. Matter 22 415501

(http://iopscience.iop.org/0953-8984/22/41/415501)

J. Phys.: Condens. Matter **22** (2010) 415501 (9pp) doi:10.1088/0953-8984/22/41/415501

First principles study of lithium insertion in bulk silicon

Wenhui Wan[1], Qianfan Zhang[1], Yi Cui[2] and Enge Wang[3,1]

[1] Institute of Physics, Chinese Academy of Sciences, Beijing 100190, People's Republic of China
[2] Department of Materials Science and Engineering, Stanford University, Stanford, CA 94305, USA
[3] School of Physics, Peking University, Beijing 100871, People's Republic of China

E-mail: egwang@pku.edu.cn

Received 30 July 2010, in final form 6 September 2010
Published 23 September 2010
Online at stacks.iop.org/JPhysCM/22/415501

Abstract

Si is an important anode material for the next generation of Li ion batteries. Here the energetics and dynamics of Li atoms in bulk Si have been studied at different Li concentrations on the basis of first principles calculations. It is found that Li prefers to occupy an interstitial site as a shallow donor rather than a substitutional site. The most stable position is the tetrahedral (T_d) site. The diffusion of a Li atom in the Si lattice is through a T_d–Hex–T_d trajectory, where the Hex site is the hexagonal transition site with an energy barrier of 0.58 eV. We have also systematically studied the local structural transition of a Li_xSi alloy with x varying from 0 to 0.25. At low doping concentration ($x = 0$–0.125), Li atoms prefer to be separated from each other, resulting in a homogeneous doping distribution. Starting from $x = 0.125$, Li atoms tend to form clusters induced by a lattice distortion with frequent breaking and reforming of Si–Si bonds. When $x \geqslant 0.1875$, Li atoms will break some Si–Si bonds permanently, which results in dangling bonds. These dangling bonds create negatively charged zones, which is the main driving force for Li atom clustering at high doping concentration.

(Some figures in this article are in colour only in the electronic version)

1. Introduction

Li ion batteries have been the most important portable power sources for consumer electronics and show great promise for vehicle electrification. One of the most important parameters for the next generation of Li ion batteries is energy density or specific energy. There has been much active research on developing high capacity lithium ion battery electrode materials [1]. Si, a well-known material used for integrated electronics and photovoltaics, can store a large number of Li atoms, and it has more than ten times the specific capacity as graphite (4200 mA h g^{-1} for the $Li_{4.4}Si$ compound, 372 mA h g^{-1} for graphite). However, there is a four-fold volume expansion that results from the alloying process which causes structural changes and mechanical breaking of Si. Recent studies on exploring a variety of nanostructured Si battery electrodes, including nanowires, core–shell nanowires, nanoparticles, nanotubes, and nanopores, show success in addressing the mechanical breaking issues [2–6]. The energetics and dynamics of Li insertion into covalently-bonded Si are critical in determining key battery performance parameters such as voltage profile, power rate, temperature effects, safety, and cyclability.

Over the past decades there has been much experimental work studying the Li insertion process. The Li diffusion rate at high temperature has been measured in bulk Si [7]. At 415 °C, the equilibrium coulometric titration curve shows that four intermediate phases exist in the Li–Si system, which are identified as $Li_{12}Si_7$, Li_7Si_3, $Li_{15}Si_4$, and $Li_{22}Si_5$ respectively [8]. Using x-ray diffraction methods, Obrovac found that the amorphization of crystalline Si could happen at room temperature [9]. Key *et al* investigated the change of local structure during the first discharge process and found that isolated Si atoms and Si–Si clusters were formed, but clusters would break apart to form isolated Si atoms when the voltage drops to 50 mV [10]. Aggarwal analyzed the excitation spectra of Li in bulk Si and Ge and concluded that the Li interstitial impurity mostly occupies the positions which

have tetrahedral symmetry [11], and the EPR experiment subsequently confirmed the conclusion [12]. The diffusion coefficient $D = D_0 \exp(-\Delta E/k_B T)$ has been measured in early research [13], and the activation energy ΔE is between 0.57 and 0.79 eV with the pre-exponential factor D_0 in the range of 1.9–9.4 $\times 10^{-3}$ cm^2 s^{-1}. An additional infrared study of localized vibrations in Si obtained local modes at 522 and 534 cm^{-1} which are attributed to the ^{7}Li and ^{6}Li isotopes in an interstitial position [14].

Redox potential is an important characteristic of anode materials in Li ion batteries. It is determined by the lithium chemical potential, which can be calculated through Monte Carlo simulations to determine the distribution of lithium ions in the host lattice of a given crystal structure [15]. However, the rate of charge and discharge in battery anodes can be limited by Li atom diffusion and mobility. Therefore, the development of new kinds of anode materials requires a comprehensive understanding of the stable configurations and diffusion modes of Li atoms in these structures. However, such information is difficult to extract from x-ray diffraction experiments directly because of the weak x-ray scattering power of the light lithium impurities within the host lattice [16]. First principles calculations, which can compute energy accurately, represent an ideal method to determine the energetics of Li impurity atoms residing in Si anode material at a microscopic level.

Previous simulations have focused on the geometry and electronic character of different Li–Si phases or amorphous phases. Density functional theory (DFT) calculations have been carried out to determine the geometry and electronic character of the compounds LiSi and $Li_{15}Si_4$ by Kubota *et al* [17, 18]. de Wijs *et al* studied the structure of $Li_{12}Si_7$ in the liquid state by analyzing the partial pair correlation functions [19]. In addition, Chevrier *et al* introduced a protocol to reproduce the charge and discharge curve of an amorphous silicon anode [20]. Milman *et al* calculated the free energy of lithium diffusion by combining *ab initio* molecular dynamics simulations with a thermodynamic integration method in which the lithium diffusion barrier in the Si lattice is about 0.58 eV [21]. DeLeo *et al* compared the hydrogen–vacancy and alkali-metal–vacancy complexes in bulk Si using a self-consistent-field scattered-wave Xα cluster method and found that Li atoms did not passivate intrinsic vacancy defects but instead provided an electron to negatively charge the vacancy [22]. Finally, Singh calculated the Li-related defects in crystalline Si using the extended Hückel theory method with and without the vacancy, but this semi-empirical method cannot relax the structure fully so the conclusion is not credible [23].

In a recent paper, we have studied Li dopants in Si nanowires [24]. Here, we will focus on the study of lithium insertion in bulk Si. We study the energetics and dynamics of Li insertion into bulk Si at different Li doping concentrations based on first principles calculations. By comparing the binding energy of a single interstitial and substitutional Li dopant at various fully relaxed positions, we find that the T_d sites are the most stable positions. The Li diffusion pathway is identified as the T_d–Hex–T_d trajectory, where the Hex site is the transition state with an energy barrier of 0.58 eV, which agrees well with experimental results. With increasing doping concentration x in Li_xSi, Li atoms tend to form clusters at concentrations as low as 0.125. The electronic structure calculations show that a new electronic state appears in the gap when the Li concentration increases, and the Li_xSi alloy becomes more metal-like.

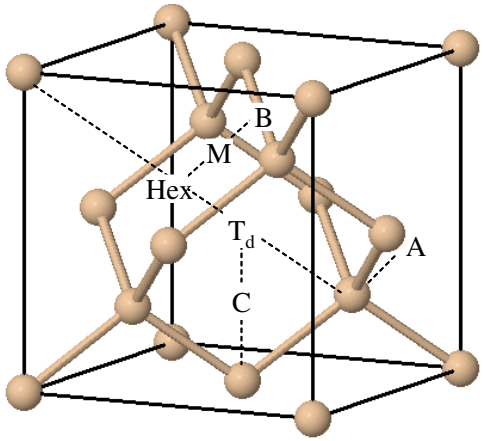

Figure 1. The T_d, Hex, A, B, C, and M sites in bulk Si with a diamond structure.

2. Simulation methods

All the DFT calculations were performed with the Vienna *ab initio* simulation package (VASP) [25, 26]. Projector augmented waves (PAW) [27] pseudo-potentials have been used to describe the interaction between electrons and ion cores. For Li atom, the Li_sv pseudo-potential treated the semi-core 1s states as valence states. For the exchange–correlation function, we have adopted a generalized gradient approximation (GGA) introduced by Perdew and Wang [28]. A plane wave basis set with an energy cutoff of 400 eV was used in all the calculations. Proper Monkhorst–Pack k-points meshes were employed for the supercells with different sizes. The structures were fully relaxed for both internal atomic coordinates and supercell shapes. The geometry optimizations were carried out until the forces on each atom were smaller than 0.01 eV Å^{-1}.

3. Single Li dopant in bulk Si

3.1. Stable position and band structure

First, we have calculated the lattice constants of bulk Si and Li as a reference point to ensure that our simulation is correct quantitatively. The obtained lattice constants are 5.46 Å and 3.53 Å for Si and Li, respectively, which agree well with the experimental values of 5.43 and 3.51 Å. Next, a single Li atom was put into a supercell with 64 Si atoms to simulate a dilute doping situation in which the Li atom can be viewed as an isolated impurity. Different nonequivalent insertion positions in the Si lattice are examined and their binding energies are calculated to extract the energetically favorable sites. These positions are shown in figure 1, which includes the tetrahedral

Table 1. The binding energies of single Li dopant in bulk Si.

Position	Binding energy (eV)
T_d	1.359
Hex	0.847
B	−1.176
S	−6.602
F	−2.392

(T_d), hexagonal (Hex), anti-bonding (A), bond-center (B), center of the second nearest silicon (C), and midway (M) sites between Hex site and B site. In addition, a substitutional (S) defect, in which a Li atom is placed on a Si lattice site, and a Frenkel defect (F), in which a Li atom is positioned on the original Si site while the Si atom is repelled to an adjacent T_d site, are also considered. Table 1 lists the calculated binding energies for all the configurations discussed above.

The binding energies at different insertion sites indicate that the Li dopant acts as an interstitial impurity rather than a substitutional one because both S and F defects lead to negative binding energies, which means the system becomes less stable after Li insertion. The T_d site is the most stable position, while the Hex site is a transition state. The relatively high energy of a Hex site compared with that of a T_d site is consistent with the early result in [21]. The B site is not a stable position as its binding energy is negative. Li defects appear on the B site only when an adjacent vacancy is present [29] at high temperature as reported in some experiments. We also calculated the energy change when a Li atom is removed from the T_d or Hex positions without relaxing the Si atoms in order to study the energy change caused by Si lattice distortion. The energy of distorted Si lattice frame for the T_d site is about 0.2 eV lower than that for the Hex site, which confirms again that Li atoms are more energetically stable in the T_d configuration.

As is shown in figure 2(a), when a Li dopant is on a T_d site, it has four nearest-neighbor Si atoms and six second nearest-neighbor Si atoms with Li–Si distances of 2.45 Å and 2.75 Å, respectively. All the neighboring Si atoms around the Li dopant move outward after structural relaxation, and the closest Si–Si bond length becomes 2.41 Å (instead of 2.37 Å in a pure Si crystal). However, the second closest Si–Si bond length shortens to 2.35 Å. When Li is on Hex site, as shown in figure 2(b), it is neighbored by six equivalent Si atoms with a Li–Si distance of 2.37 Å. The nearest Si–Si bond length expands to 2.47 Å and the second nearest length shortens to 2.34 Å. We also find that the potential energy surface near the T_d site is very flat insider the space formed by four closed six atomic rings of Si atoms in figure 2(a). That means the Li atom can move around the T_d site easily at room temperature as long as it does not get near to Hex site considering its inherent oscillation energy of about 65 meV [11].

The electronic band structures for bulk Si with a Li dopant located on the T_d and Hex sites are displayed in figures 3(b) and (c) respectively, while the electronic band structure of pure Si is shown in figure 3(a) for comparison. We can see that when Li is introduced, the shape of band structure does not change much but the Fermi level is moved to the bottom of conduction band, which indicates that the Li-doped Si material is metal-like. The Li impurity donates its partial 2s electron to Si but

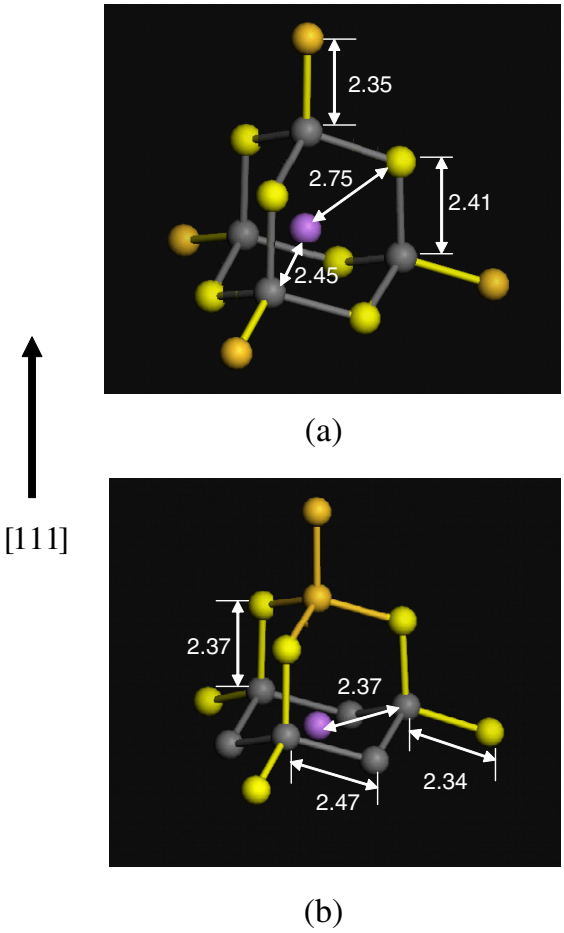

Figure 2. Illustration of the ring Si atoms and Si–Si bonds around a single Li atom when the Li atom is on the T_d site (a) and the Hex site (b). The purple atom is the Li atom, the gray atoms and bonds are its nearest Si atoms and Si–Si bonds, the yellow atoms and bonds are its second nearest Si atoms and Si–Si bonds, and the remaining atoms are other Si atoms in the bulk. The unit of distance is Å.

does not create an extra level around the band gap. It can also be seen that the ionized energy of the Li 2s electron is about zero, not the 33 meV reported in experiments [30, 31]. This distinction comes from the underestimation of the band gap by DFT study. The charge redistribution caused by the Li dopant can clearly be seen from the charge density difference on the plane containing Li and neighbor Si atoms, which is shown in figure 4. The graphic is based on the formula:

$$\Delta\rho = \rho(\mathrm{Li+Si}) - \rho(\mathrm{Si}) - \rho(\mathrm{Li}) \qquad (1)$$

where $\rho(\mathrm{Li+Si})$, $\rho(\mathrm{Si})$, $\rho(\mathrm{Li})$ are the electron densities of the Si–Li system, pure bulk Si and a single Li atom. For both cases of a Li dopant on T_d and Hex sites, electron density around the Li atom decreases while that in the Li–Si bond increases, which clearly indicates the partial electron drifts from the Li dopant toward its neighboring Si atom. However, the electron density among the neighboring Si–Si bond reduces because the length of the Si–Si bond extends and the interaction weakens as discussed above.

The total density of states (DOS) and the partial density of states (PDOS) for different atoms are shown in figure 5.

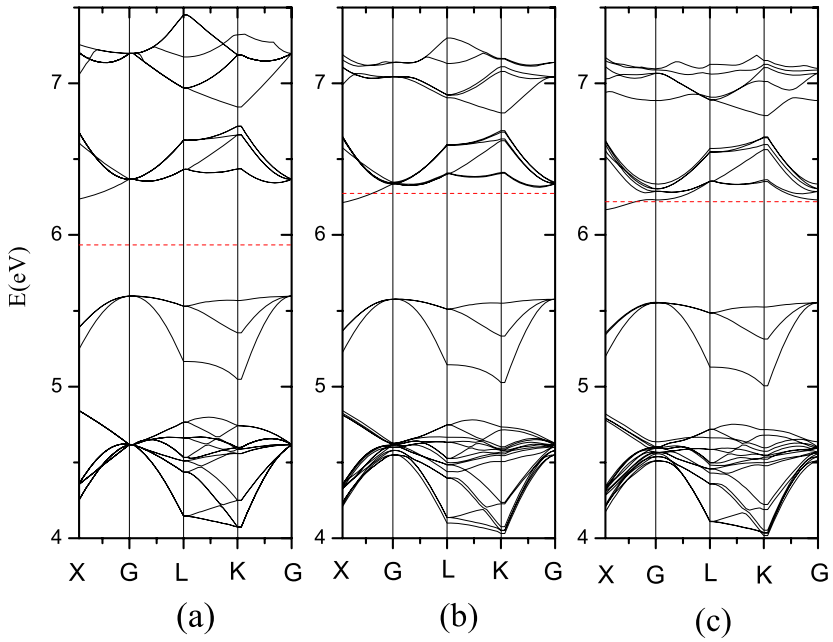

Figure 3. The band structures of bulk Si (a) and bulk Si with a Li dopant located on the T_d site (b) and on the Hex site (c). The dashed line is the position of the Fermi energy, which is 6.43 eV and 6.39 eV for Li located on T_d and Hex sites, respectively.

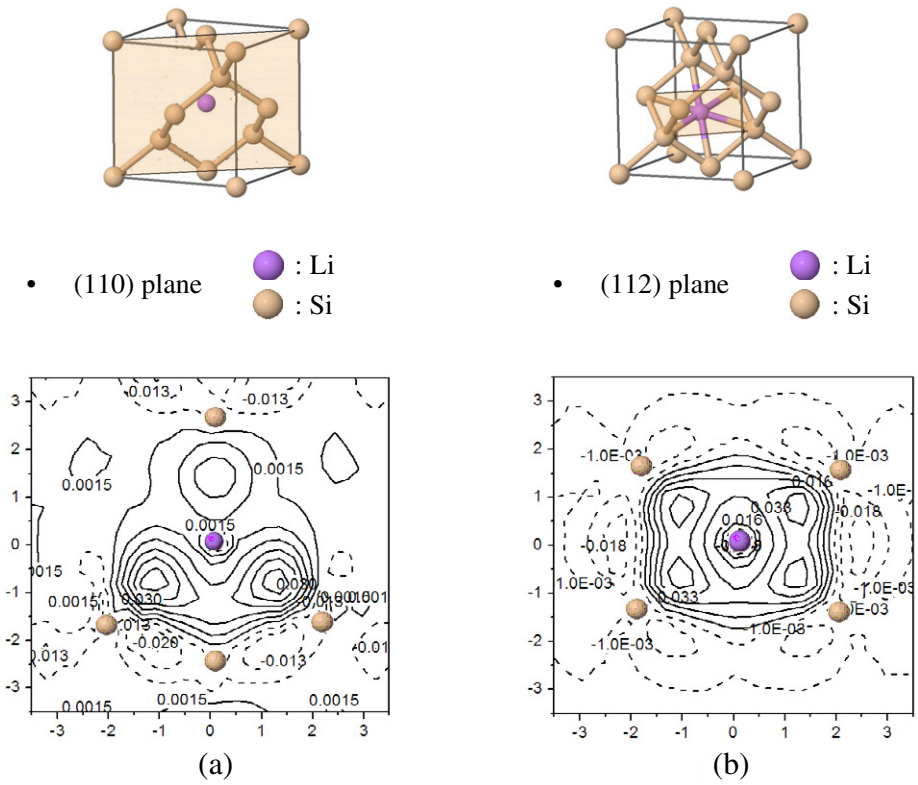

Figure 4. The charge density difference on plane (110) when Li dopant is on the T_d site (a) and on plane (112) when Li dopant is on the Hex site (b). The yellow ball is a Si atom and the purple one is a Li dopant. The coordinate unit is Å and the unit of charge density is e Å^{-2}.

The top window displays the total DOS, while the middle and bottom windows show the PDOS around a Li dopant and one of its neighboring Si atoms, respectively. The s (p) component is depicted in a black (red) line. The DOS related to the Li 1s orbital is not shown here because it is located at the low energy region around −50 eV and has no influence on the Li–Si interaction. The shape of the DOS is almost the same as that of bulk Si since the total DOS mainly comes from the Si atoms

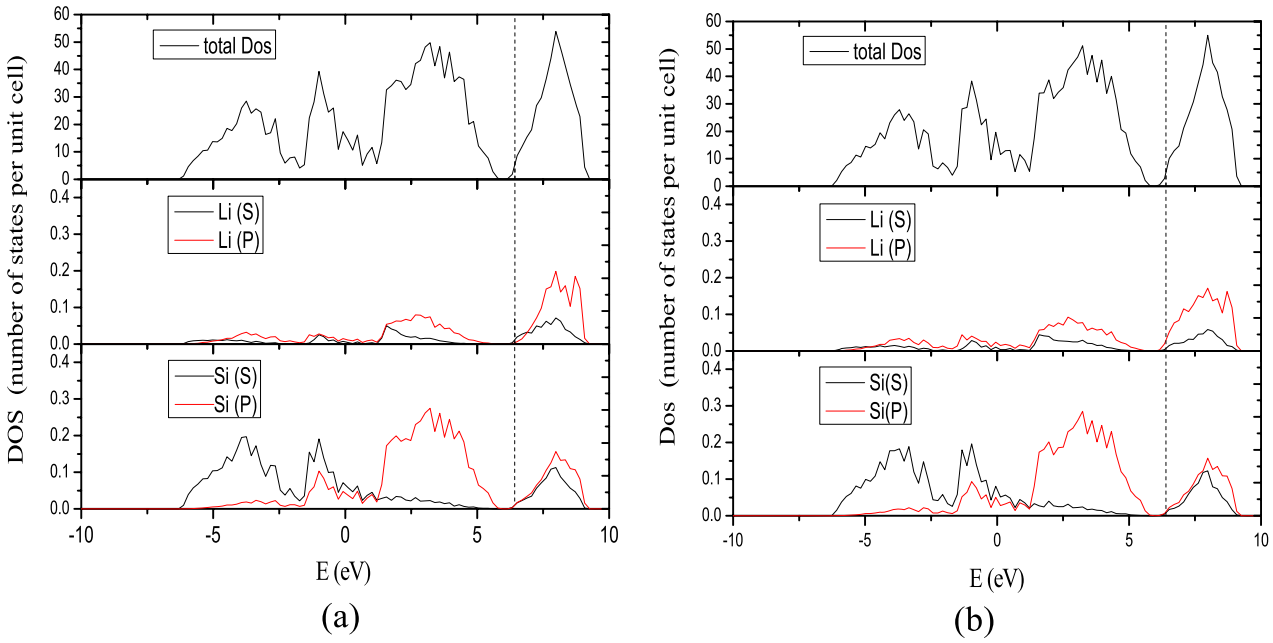

Figure 5. The PDOS of the Si supercell with Li occupying the (a) T_d and (b) Hex sites. The dashed line here is the position of Fermi energy, whose values are 6.43 eV and 6.39 eV for Li located at the T_d and Hex sites, respectively.

and the host lattice changes little after Li doping. The Fermi energy is higher when the Li defect is located on the T_d site. The integral of the Li DOS shows that more electrons donate to bulk Si when a Li atom is on a T_d site, which indicates again the stronger interaction between a Li dopant on a T_d-site and its neighboring Si atoms. A Li defect makes two main contributions to the total DOS; one is located among the valence band while the other is near the Fermi level, which can be viewed as bonding and anti-bonding states introduced by doping. In particular, the Li PDOS contains non-zero p components whose range is almost the same as the p orbit of Si atoms, and the p component is even larger than the s component. Therefore, it is clear that the p component of a Li dopant is caused by the hybridization between the original Li 2s orbital and Si 3p orbital.

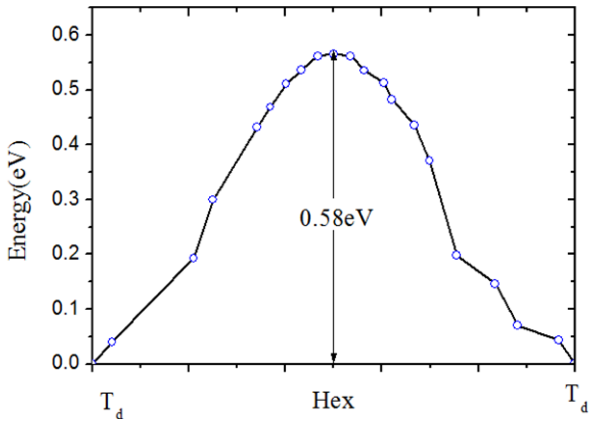

Figure 6. Diffusion energy for a Li dopant along the T_d–Hex–T_d diffusion pathway.

3.2. Diffusion of a Li dopant

Based on the energy calculation of different Li doping sites, it can be obtained that the direct diffusion pathway is through a T_d–Hex–T_d trajectory. We have calculated the diffusion barriers using the NEB method [32, 33] by relaxing various configurations between the starting and ending points along the diffusion pathway. The energy curve for Li diffusion between the adjacent T_d sites is presented in figure 6. The barrier height is about 0.58 eV, which is in good agreement with existing theory [21] and experiment (0.57–0.79 eV) [13]. The Hex site is confirmed to be a saddle point along the migration pathway. As displayed in figure 1, when a Li defect reaches the T_d site through the T_d–Hex–T_d pathway and continues to move along [111] direction, it will be repelled by a host Si atom. As a result, it has to switch its diffusion direction to another [111] direction, and the long-range diffusion processes occurs in a manner that we can call 'zig-zag' fashion.

Furthermore, we find that Li diffusion is quite different from H diffusion in bulk Si. Besides neutral Li, we have also calculated diffusion paths of positively charged Li^+ and negatively charged Li^-. To our surprise, both Li ions with positive and negative charge prefer to stay at the T_d site and the Hex site, and the diffusion path is again along the T_d–Hex–T_d trajectory. However, the positive and neutral hydrogen impurity diffuses in bulk Si along a B–B trajectory, where the transition state is near the C site. The diffusion path for a negative hydrogen defect is along the T_d–Hex–T_d line, which is the same as in the Li case [34, 35]. The site preference of a dopant in bulk Si is the result of a competition between the energy ascent due to the distortion of the closest Si shell around the defect and the energy descent due to attractive interaction stemming from electron transfer between the impurity and its neighboring Si atoms. Both H and Li atoms have one valence

electron, but they have a large difference in ionic radius. A Li atom has a much larger radius compared with a H atom or H^+ ion, and as a result, it will stay further away from the host atoms in closely-packed Si bulk. That is the main reason why a Li dopant takes the T_d and Hex sites as the stable and transition sites; these sites have Si–Li bond lengths that are the longest and the second longest, respectively. It may also explain why H^- follows a similar diffusion pathway to a Li dopant, because it has a larger radius compared to H or H^+.

4. Li dopants in bulk Si: different doping concentrations

When the doping concentration increases, the simplest scheme is that Li impurity atoms will continuously occupy the T_d sites until no T_d voids are available in bulk Si. It means that the undestroyed host lattice can retain a ratio of [Li]/[Si] from $x = 0$–1, because the number of T_d sites is equal to that of Si atoms in a bulk Si unit cell. However, according to charge–discharge experiments by Limthongkul [36], it was shown that amorphization occurs at a ratio of [Li]/[Si] as low as 0.1. Therefore, the Si–Si bond may be broken at a certain low Li doping concentrations. In the following discussion, we will focus on the most stable configurations for different Li doping concentrations and investigate the critical point when Li impurities prefer to gather and form clusters.

By inserting more Li atoms into Si supercells, we have simulated the Li_xSi alloys at $x = 0.031\,25$, 0.0625, 0.125, 0.1875, and 0.25. For each x value, a number of initial geometrical configurations are considered and are fully relaxed to the distinct stable structures. By comparing the energy of the obtained stable structures, we finally select the one corresponding to the lowest energy for each doping concentration under study.

4.1. Low doping region ($x = 0.0315$, 0.0625)

When $x \leqslant 0.0625$, the most stable configuration is that both Li atoms are located on the T_d sites. The further the distance between them, the lower energy the structure has, as displayed in figure 7(a). This agrees with the situation of dilute doping concentration. The distance between two nearest T_d sites is 2.61 Å, which is smaller than a Li–Li bond length of 3.05 Å in Li metal. So if Li atoms occupy two adjacent T_d sites they will repel each other. Therefore, Li dopants are inclined to form isolated impurities in bulk Si at very low doping concentrations, which results in a homogeneous distribution.

This can be further understood by studying the dynamics of the process. We find that the Li diffusion is accelerated when Li defects are closely situated in a very low concentration case. We design a diffusion pathway where one Li atom is fixed and the other one diffuses along the T_d–Hex–T_d pathway. The distance between the two Li atoms becomes longer and longer as the diffusion proceeds. Figure 7(b) shows the energy as a function of distance along the pathway. When another Li atom occupies the adjacent T_d site, the Li diffusion barrier of the T_d-to-T_d process is about 0.1 eV lower than that of an isolated Li dopant. This can be viewed as an example of cooperative diffusion, in which the diffusion occurs with a lower energy barrier when two Li atoms are placed closely in the low doping regime.

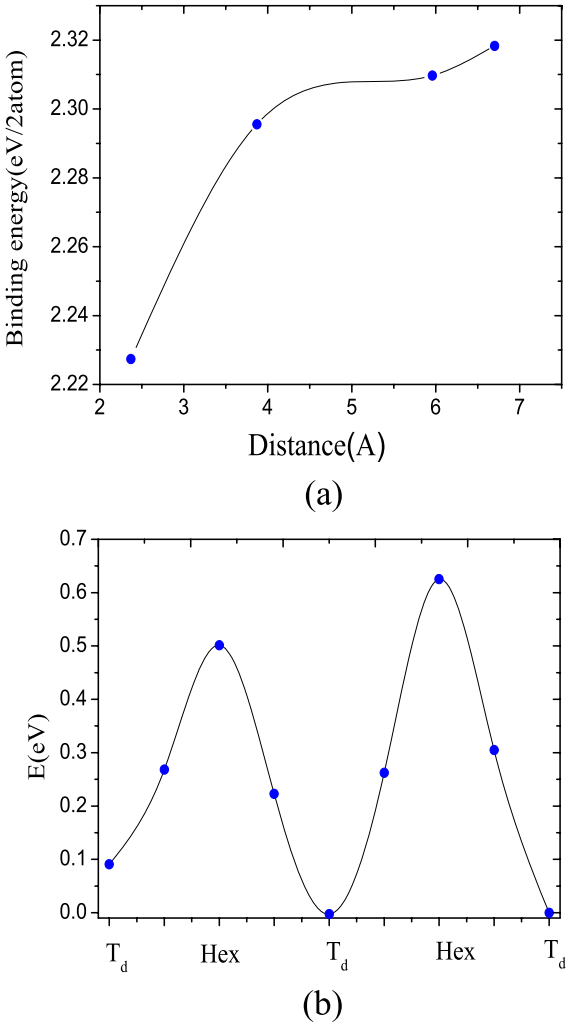

Figure 7. (a) The binding energy of a configuration in which two Li atoms occupy the T_d sites as a function of distance between them when $x \leqslant 0.0625$. (b) Diffusion energy barrier along a normal Li pathway when another Li atom occupies the adjacent T_d site.

4.2. Intermediate doping region ($x = 0.125$)

When more Li dopants are added into bulk Si, a clear local structure distortion occurs at $x = 0.125$. The most stable configuration (labeled as q_S) is displayed in figure 8, whose energy is 0.52 eV lower than the metastable configuration in which all the Li atoms stay at T_d sites (labeled as q_M). The obtained stable structure causes a local distortion of the host lattice, which destroys the homogeneous arrangement of the six-member ring in perfect crystalline Si. One five-member ring and one seven-member ring appear around the Li dopants.

To study the dynamic process of the lattice distortion, we have calculated the migration pathway from the q_M structure to the q_S structure, as shown in figure 8. The migration barrier from q_M to q_S is about 0.69 eV, which is not very high. Therefore, in light of the dynamics, Si–Si bonds can be

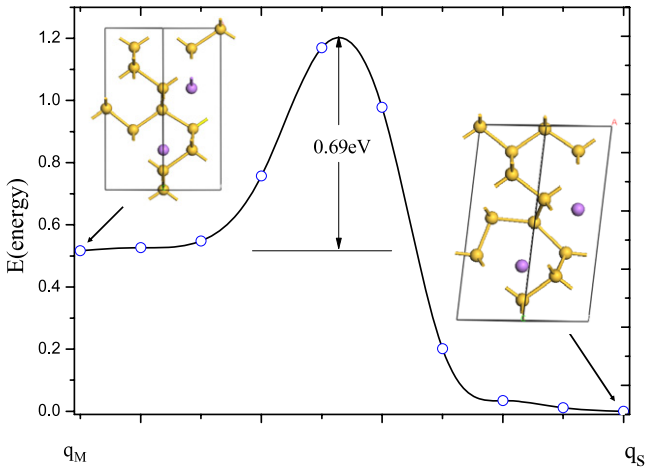

Figure 8. The calculated total energy profile along the q_M to q_S transformation pathway at the doping concentration of $x = 0.125$. The structures q_M and q_S, used in the NEB calculation, are also given here.

broken and reformed frequently at $x = 0.125$, which cannot be observed at lower Li doping concentrations.

4.3. High doping region ($x = 0.1875, 0.25$)

As the doping concentration increases to 0.1875 or above, the host lattice is significantly destroyed with respect to its diamond-cubic symmetry as well as short-range order. A typical distorted structure with the lowest energy is shown in figure 9(b) after full relaxation. A set of letters is used to label the Si and Li atoms. We can see clearly that the Si(A)–Si(B) and Si(C)–Si(D) bonds are broken and a new Si(B)–Si(D) bond forms. Meanwhile, the distance between Si(A) and Si(C) is 3.308 Å, which is too long to represent a bond. Therefore, the three-Si-neighbored Si(A) or Si(C) atoms have a dangling bond and create a negatively charged environment around them. As a result, the Li impurities close to that site will be ionized by electron transfer and attracted to the negatively charged zone. The strong attractive interaction between a negative Si ion and a positive Li ion compensates for the increase in energy caused by the distortion of the Si lattice. On the other hand, the diffusion of a Li dopant in bulk Si at high doping concentration will be different from the isolated case and may be mediated by the lattice distortion of bulk Si.

4.4. Li atom clustering

A coordinate number n_{SiLi}, the number of Li atoms around a Si atom, is introduced to study dopant clustering. We employ r_c as the cutoff radius to judge whether Si is neighbored by Li dopants. r_c is chosen as the middle between the first and second peak in a Si–Li pair correlation function g_{SiLi}, which is defined as:

$$g_{\mathrm{SiLi}}(r) = \frac{V}{4\pi r^2 N_{\mathrm{Si}} \mathrm{d}r}\,\mathrm{d}n_{\mathrm{Li}}. \qquad (2)$$

Here N_{Si} is the total number of Si atoms in the supercell, V is the volume of the supercell, and $\mathrm{d}n_{\mathrm{Li}}$ is the number of Li atoms within a distance between r and $r + \mathrm{d}r$ from a given Si atom. Using the r_c obtained above, we have calculated the coordinate number lists n_{SiLi} of all the Si atoms. Due to temperature effects, the reasonable distribution of a Li coordinate number was obtained by averaging over all the considered stable and metastable structures under the Boltzmann statistic principle, which is carried out at 300 K.

We show the ratio of Si atoms neighbored by (a) zero, (b) one, (c) two, and (d) three Li atoms at $x = 0.031\,25$, 0.0625, 0.125, 0.1875, and 0.25 in figure 10. One can see the proportion of Si atoms that has no neighboring Li atoms decreases significantly with increasing x. Meanwhile, the number of Si atoms that connect to two Li atoms increases markedly. This can be explained by the existence of dangling bonds. Breaking a single Si–Si bond will provide two dangling bonds. The extra local electrons produce a negatively charged zone, and two vicinal Li atoms will donate their 2s electrons to the local electronic state of these Si atoms and Si–Li bonds are formed. However, as soon as the Si dangling bonds are saturated by Li atoms, the further attraction of additional Li atoms weakens. Therefore, the proportion of Si connected to three Li atoms does not greatly increase as the doping concentration grows.

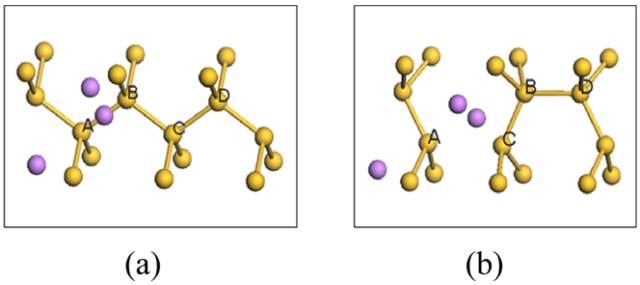

Figure 9. Rearrangement of the Si lattice after lithium insertion at the doping concentration of $x = 0.1875$. (a) is the Si structure before relaxing; (b) is the Si configuration after geometrical relaxation. The purple balls represent Li atoms and the yellow ones are Si atoms. A similar situation occurs at $x = 0.25$.

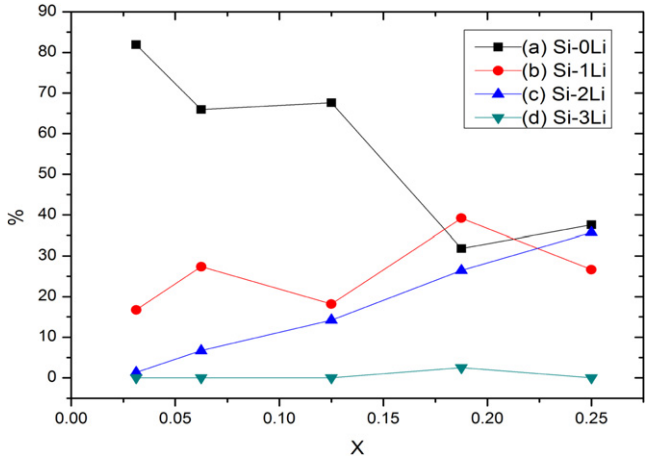

Figure 10. Proportion of a Si atom with different Li coordinate number plotted as a function of x in a $\mathrm{Li}_x\mathrm{Si}$ supercell. Here (a), (b), (c) and (d) are referred to as Si atoms connected to zero, one, two, and three Li atoms, respectively.

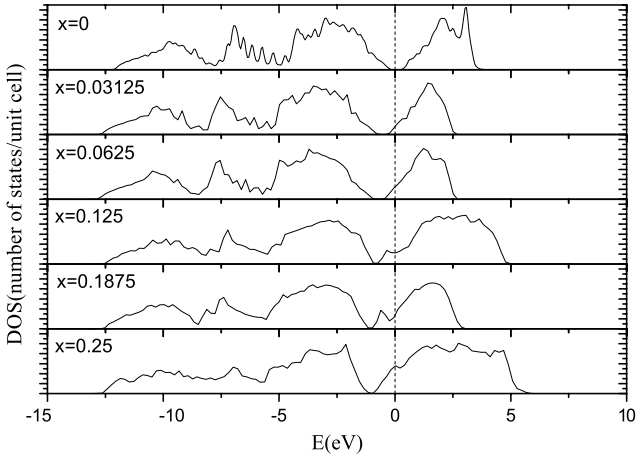

Figure 11. Density of states of Li_xSi at different doping concentrations. From top to bottom the x value is (a) 0, (b) 0.031 25, (c) 0.0625, (d) 0.125, (e) 0.1875, and (f) 0.25. The dashed line is labeled as the Fermi energy.

To summarize the discussion above, we have seen that Li atoms incline to separate from each other when $x < 0.125$. A homogeneous doping distribution is expected. When $x = 0.125$, Li atoms tend to cluster, which is induced by a local lattice distortion with frequently breaking and reforming of Si–Si bonds. Our study shows that, at $x = 0.1875$, a Li ion pair appears near a permanently broken Si bond with a Li–Li distance of 2.92 Å, which is close to the Li bond length of 3.06 Å in bcc Li metal. This is because the dangling bonds create a negatively charged zone, which is the main driving force for Li atom clustering at high doping concentrations of $x \geqslant 0.1875$.

4.5. Density of states

To understand the electronic properties of Li_xSi alloys, we have calculated the density of states (DOS) at different doping concentrations between $x = 0$ and 0.25. The DOS profiles are displayed in figure 11. The band gap of bulk Si is 0.6 eV by our calculation. The Fermi energy lies in the middle of the gap. As the Li defects are inserted into bulk Si, extra electrons are donated into the host lattice and the Fermi energy shifts to the bottom of the conduction band. At the same time, the band gap narrows gradually. When $x = 0.125$, a new electronic state appears near the Fermi energy as shown by a small peak. The peak becomes clearer with continuously increasing x up to 0.1875. As more Li atoms are inserted, for example when $x = 0.25$, the DOS at the Fermi level greatly increases and the boundary between the new state and the conduction band bottom disappears. The resulted Li–Si alloy shows metallic behavior.

5. Conclusion

In summary, we have investigated the energetics and dynamics of Li dopants in bulk Si by first principles calculations at the atomic level for different impurity concentration. By comparing the different Li insertion sites in Si, we have found that a Li dopant acts more like an interstitial shallow donor than a substitutional one. In addition, the T_d site is the most stable site and the Hex site is a transition state. The diffusion of a Li atom is through a T_d–Hex–T_d trajectory with a barrier of 0.58 eV. At low doping concentrations, Li atoms prefer to separate from each other as far as possible to form a homogeneous doping distribution. The hybridization makes the s electron of Li transfer to the p orbital. When increasing the concentration to $x = 0.125$, Li dopants change behavior from repelling each other to gathering together; this is induced by a lattice distortion with frequent breaking and reforming of Si–Si bonds. When $x \geqslant 0.1875$, Li dopants will break a Si–Si bond permanently to result in two dangling bonds. These dangling bonds create a negatively charged zone that attracts two nearby Li ions. Further detailed analysis of the DOS shows that a new state appears in the band gap of bulk Si in the doping regime between $x = 0.125$ and 0.1875. This impurity band merges with the bottom of the conduction band at high doping concentrations. Then Li_xSi alloy then shows metallic behavior. Our study presents a local structural phase transition during Li insertion. More interestingly, clear Si lattice distortion and Li dopant clustering appear at quite low doping concentrations. These results reveal the fundamental mechanics of Li-doped Si alloys, and may provide a guide for further experimental study.

Acknowledgments

This work was supported by CAS and NSFC. EW acknowledges Stanford GCEP visiting scholar program and KITP at UCSB. We also gratefully acknowledge the computational time by the Swedish agency SNAC. YC acknowledges support from the King Abdullah University of Science and Technology (KAUST) Investigator Award (No. KUS-l1-001-12), Stanford GCEP and US ONR.

References

[1] Tarascon J M 2010 *Nat. Chem.* **2** 510
[2] Chan C K, Peng H, Liu G, Mcilwrath K, Zhang X F, Huggins R A and Cui Y 2008 *Nat. Nanotechnol.* **3** 31–5
[3] Cui L F, Ruffo R, Chan C K, Peng L and Cui Y 2009 *Nano Lett.* **9** 491–5
[4] Gao B, Sinha S, Fleming L and Zhou O 2001 *Adv. Mater.* **13** 816–9
[5] Moradian R, Behzad S and Chegel R 2009 *Phys. Lett.* A **373** 2260–6
[6] Kang D K, Corno J A, Gole J L and Shin H C 2008 *J. Electrochem. Soc.* **155** A276–81
[7] Pell E M 1960 *J. Appl. Phys.* **31** 291–302
[8] Wen C J and Huggins R A 1981 *J. Solid State Chem.* **37** 271–8
[9] Obrovac M N and Christensen L 2004 *Electrochem. Solid-State Lett.* **7** A93–6
[10] Key B, Bhattacharyya R, Morcrette M, Seznéc V, Tarascon J M and Grey C P 2009 *J. Am. Chem. Soc.* **131** 9239–49
[11] Aggarwal R L, Fisher P, Mourzine V and Ramdas A K 1965 *Phys. Rev.* **138** A882–93
[12] Watkins G D and Ham F S 1970 *Phys. Rev.* B **1** 4071–98
[13] Canham L T 1988 *Properties of Silicon* (*Electronic Materials Information Service (EMIS) Datareviews Series No. 4*) ed K V Ravi, N Hecking, W Fengwei, Z Xiangqin and L N Alexsandrev (London: INSPEC) p 455

[14] Balkanski M and Nazarewicz W 1966 *J. Phys. Chem. Solids* **27** 671–84
[15] Reimers J N and Dahn J R 1993 *Phys. Rev.* B **47** 2995–3000
[16] Arrouvel C, Parker S C and Islam M S 2009 *Chem. Mater.* **21** 4778–83
[17] Kubota Y, Escaño M C S, Nakanishi H and Kasai H 2008 *J. Alloys Compounds* **458** 151–7
[18] Kubota Y, Escaño M C S, Nakanishi H and Kasai H 2007 *J. Appl. Phys.* **102** 053704
[19] De Wijs G A, Pastore G, Selloni A and van der Lugt W 1993 *Phys. Rev.* B **48** 13459–68
[20] Chevrier V L and Dahn J R 2009 *J. Electrochem. Soc.* **156** A454–8
[21] Milman V, Payne M C, Heine V, Needs R J, Lin J S and Lee M H 1993 *Phys. Rev. Lett.* **70** 2928–31
[22] DeLeo G G, Fowler W B and Watkins G D 1984 *Phys. Rev.* B **29** 1819–23
[23] Singh V A, Weigel C and Corbett J W 1980 *Phys. Status Solidi* b **100** 533–9
[24] Zhang Q F, Zhang W X, Wan W H, Cui Y and Wang E G 2010 *Nano Lett.* **10** 3243–9
[25] Kresse G and Hafner J 1993 *Phys. Rev.* B **48** 13115–8
[26] Kresse G and Furthmüller J 1996 *Phys. Rev.* B **54** 11169–86
[27] Blöchl P 1994 *Phys. Rev.* B **50** 17953–79
[28] Wang Y and Perdew J P 1991 *Phys. Rev.* B **44** 13298–307
[29] Wahl U, Restle M, Ronning C, Hofsäss H and Jahn S G 1994 *Phys. Rev.* B **50** 2176–80
[30] Keffous A, Hadjersi T, Cheriet A, Bourenane K, Gabouze N, Boukennous Y, Kezzoula F, Zitouni M A and Menari H 2006 *Vacuum* **81** 417–21
[31] Vanfleet H B, Decker D L and Curtin H R 1972 *Phys. Rev.* B **5** 4849–56
[32] Mills G and Jónsson H 1994 *Phys. Rev. Lett.* **72** 1124–7
[33] Jonsson H, Mills G and Jacobsen K W 1998 *Classical and Quantum Dynamics in Condensed Phase Simulations* (Singapore: World Scientific) chapter 16
[34] Chang K J and Chadi D J 1989 *Phys. Rev.* B **40** 11644–53
[35] Van de Walle C G, Denteneer P J H, Bar-Yam Y and Pantelides S T 1989 *Phys. Rev.* B **39** 10791–808
[36] Limthongkul P, Jang Y I, Dudney N J and Chiang Y M 2003 *J. Power Sources* **119** 604–9